

## CENTRAL ENGINES OF ACTIVE GALACTIC NUCLEI: PROPERTIES OF COLLIMATED OUTFLOWS AND APPLICATIONS FOR COSMOLOGY

ERICK J. GUERRA AND RUTH A. DALY<sup>1</sup>

Department of Physics, Joseph Henry Laboratories, Princeton University, Princeton, NJ 08544

Received 1996 September 13; accepted 1997 September 8

### ABSTRACT

Powerful extended radio galaxies in the 3CR sample are observed out to redshifts of about 2. For redshifts greater than 0.3, the average lobe-lobe size of these sources decreases monotonically with redshift for all reasonable cosmological parameter choices. This suggests that the characteristic time for which an active galactic nucleus (AGN) produces highly collimated outflows that power radio emission is shorter for high-redshift sources than it is for low-redshift sources. The analysis presented here supports this conclusion.

The relation between the active lifetime and the beam power of powerful extended radio galaxies is investigated here. It is found that the data are accurately described by a model in which the active lifetime of the source,  $t_*$ , is written as a power law in the energy extraction rate,  $L_j$ . The exponent of the power law is estimated to be  $\beta \simeq 2.1 \pm 0.6$ , where  $\beta$  is defined by  $t_* \propto L_j^{-\beta/3}$ . Note that the value of  $\beta$  for an Eddington-limited system of zero is excluded by this analysis. The fact that  $\beta$  is constrained to lie within a certain range may be used to constrain models of large-scale jet production and cosmological parameters.

The comparison of the redshift evolution of characteristic source sizes with the average lobe-lobe size for powerful extended 3CR radio galaxies can be used to constrain cosmological parameters if three empirically estimated quantities can be accurately determined for a subset of the sources. This method of using radio sources as a modified standard yardstick is very similar to the use of supernovae as a modified standard candle. As discussed here, one observable quantity, the lobe propagation velocity, is beset by potential biases that are not completely understood. The analysis presented here shows that these biases do not significantly affect the results on  $\beta$  but must be studied in more detail before cosmological parameters can be estimated precisely. Allowing for the potential biases mentioned above, best fits of the data yield a low value of  $\Omega_0$ , which is about  $2\sigma$  away from a flat, matter-dominated universe.

*Subject headings:* cosmology: observations — galaxies: active — galaxies: evolution — galaxies: jets — radio continuum: galaxies

### 1. INTRODUCTION

Active galactic nuclei (AGNs) appear in a variety of forms that include powerful radio emitters produced by highly collimated outflows. The mechanism(s) that produces these outflows is(are) not known, though several models have been suggested (see, e.g., Blandford & Znajek 1977; Blandford & Payne 1982; Wilson & Colbert 1995; Lightman & Eardley 1974; Rees et al. 1982; Narayan & Yi 1994, 1995).

Powerful extended radio galaxies can be used to probe AGN central engines, as described here and by Daly (1994, 1995). Radio sources are referred to as “powerful” if their radio powers at 178 MHz satisfy  $P_{178} \gtrsim 3 h^{-2} \times 10^{26}$  W Hz<sup>-1</sup> sr<sup>-1</sup>, assuming a deceleration parameter  $q_0 = 0$  and parameterizing Hubble’s constant in the usual way:  $H_0 = 100 h$  km s<sup>-1</sup> kpc<sup>-1</sup>. These sources are all on the FR II (edge-brightened) side of the FR I–FR II break defined by Fanaroff & Riley (1974). They are “extended” because their core-lobe separations range from about  $25 h^{-1}$  kpc to  $240 h^{-1}$  kpc (e.g., the radio galaxies listed by Wellman, Daly, & Wan 1997a, 1997b; hereafter WDW97a and WDW97b), which indicate that the outflows are interacting with intergalactic or intracluster gases. Only galaxies, and no quasars, are considered here to minimize projection effects, since it is widely believed that powerful extended radio galaxies have

lobes and bridges that lie closer to the plane of the sky than those of quasars (see § 3.1 below, and Wan & Daly 1998a).

One key to the properties of collimated outflows is the relation between the rate at which energy is channeled into the outflow, known as the beam power or luminosity in directed kinetic energy, and other parameters such as the total time the outflow exists, and the energy available to power the outflow. In an Eddington-limited system, the rate of energy extraction,  $L_E$ , is proportional to the mass of the central compact object,  $M$ . Since the energy available to power the source is equal to the mass of the central compact object times the emission/accretion efficiency,  $E \simeq \eta M$ , the total time the outflow exists is  $t_E \simeq E/L_E \propto \eta M/M \propto \eta$ . Thus, the total time the outflow exists for an Eddington-limited system depends only on  $\eta$ , and not explicitly on  $L_E$  or  $E$ .

The relation between the beam power and the total time an AGN produces collimated outflows is empirically investigated here for the case of powerful extended radio galaxies. The data can be understood if the total time the AGN produces collimated outflows depends on the beam power, and thus, the outflows are not Eddington-limited systems. The empirical relations obtained here can be used to constrain models of energy extraction from AGNs and may provide insight on the conditions at the very core of AGNs.

The method and model described here can be used to constrain cosmological parameters if the redshift behavior of empirically determined quantities can be estimated to

<sup>1</sup> National Young Investigator.

relatively high accuracy (Daly 1994). The constraints on cosmological parameters that can be placed with the existing data are described in § 5. Modest constraints (i.e., about  $2\sigma$ ) on a flat, matter-dominated universe may be placed at the present time. More precise constraints can be placed when the lobe propagation velocity is determined more accurately or can be estimated more directly. As described in § 4.3, uncertainties that affect the lobe propagation velocity do not affect, within the errors, the estimate of the model parameter  $\beta$ , which relates the beam power and the total time an AGN produces collimated outflows. It should be noted that this method of using radio sources as a modified standard yardstick is similar to the use of supernovae as a modified standard candle (see, e.g., Perlmutter et al. 1997; Garnavich et al. 1997).

A basic model that describes the observed characteristics of powerful extended radio sources rather well is presented in § 2. The radio source samples used in the present study, including their limitations, are described in § 3. The application of the data to the model, and constraints on the relation between the beam power and the time for which the outflow occurs, are detailed in § 4. The use of current data to estimate and constrain cosmological parameters is discussed in § 5. A general discussion follows in § 6.

## 2. A MODEL OF THE LOBE SEPARATION IN POWERFUL EXTENDED RADIO SOURCES

### 2.1. Foundations of the Model

The foundation of a model that describes the lobe separation of powerful extended radio sources is discussed in detail by Daly (1994, 1995). Powerful extended radio sources have regular, straight bridges and lobes that are thought to propagate supersonically outward into the ambient gas surrounding them (Leahy & Williams 1984, hereafter LW84; Alexander & Leahy 1987, hereafter AL87). The lobe propagation velocities are computed on the basis of spectral aging along the bridges (see, e.g., Myers & Spangler 1985; Leahy, Muxlow, & Stephens 1989, hereafter LMS89; WDW97a, WDW97b).

It should be noted that results from standard spectral aging have been criticized recently (Katz-Stone, Rudnick, & Anderson 1993; Rudnick, Katz-Stone, & Anderson 1994; Rudnick & Katz-Stone 1996; Eilek & Arendt 1996; Eilek 1996). These authors have argued that synchrotron aging may not be the correct or only explanation for the spectral curvature observed in the bridges of extended radio sources. Until more conclusive data are obtained to settle this controversy, we adopt the practice of using lobe velocities from spectral aging analysis since WDW97b find that these velocities and the inferred surrounding gas temperatures agree well with results from lobe asymmetry analysis and X-ray observations.

WDW97a find the data agree well with a model in which the bridges of these sources expand laterally and the plasma inside undergoes adiabatic expansion. Their analysis suggests that the backflow velocity of the plasma within the bridge is small compared to the lobe advance velocity and can be neglected. It should be noted that backflow can be negligible along quiescent bridges but significant near the hot spot, in agreement with numerical simulations (see, e.g., Norman 1996).

The ambient gas density around the lobes of powerful extended radio sources can be estimated on the basis of ram pressure confinement since the lobes propagate supersoni-

cally (see, for example, Daly 1994, 1995; WDW97b). It can be shown that the number density of the ambient gas,  $n_a$ , is given by

$$n_a \propto f(b) \frac{B_{\min}^2}{v_L^2}, \quad (1)$$

where  $v_L$  is the lobe propagation velocity;  $B_{\min}$  is the minimum energy magnetic field;  $b$  is the offset of the lobe magnetic field,  $B_L$ , from minimum energy magnetic field ( $B_L = bB_{\min}$ ); and  $f(b) = (4/3)b^{-3/2} + b^2$ . WDW97a compute values of  $b$  for Cygnus A by comparing their estimates of pressure in the lobes, pressure in the bridge, and Mach number of lobe advance to estimates based on X-ray observations of gas density, thermal pressure, and temperature of the surrounding ambient gas. In particular, each of these three independent estimates gives  $b \simeq 0.25$  for Cygnus A (see § 3.2.1), in agreement with the result of Carilli et al. (1991). WDW97b show that the source to source dispersion in  $b$  must be rather small, less than about 15%.

Daly (1990) derives an expression for the beam power or the luminosity in directed kinetic energy,  $L_j$ , by equating the work done by the lobe while it propagates into the ambient gas to the energy supplied by the collimated outflow:

$$L_j \propto n_a a_L^2 v_L^3 \propto (v_L/k)^3, \quad \text{where } k \equiv (n_a a_L^2)^{-1/3} \quad (2)$$

and  $a_L$  is the lobe width. It should be noted that the typical  $L_j$  for radio galaxies in the sample examined below (§ 3.2) is about  $10^{45}$  ergs  $s^{-1}$  assuming  $b = 0.25$ , and it appears that  $L_j$  is time independent for a given source (Wan, Daly, & Wellman 1996; Wan & Daly 1998c). For a roughly constant  $L_j$ , the energy supplied by the central engine to power the collimated outflows is  $E_i \sim L_j t_*$ , where  $t_*$  is the lifetime of the collimated outflows. For  $t_*$  between  $10^7$  and  $10^8$ , which agrees with spectral aging (see, e.g., AL87; LMS89; Liu, Pooley, & Riley 1992, hereafter LPR92), the energy supplied by the central engine is  $E_i \simeq 10^{60}$  ergs  $\simeq 10^6 M_\odot c^2$ . For emission/accretion efficiencies of 0.01–0.1, the mass of the central compact object would be  $10^7 M_\odot$ – $10^8 M_\odot$  which is similar to those discussed in models of jet formation in powerful FR II galaxies (see, e.g., Wilson & Colbert 1995).

### 2.2. Relation between Active Lifetime and Beam Power

The data clearly show that the average lobe-lobe size of powerful extended 3CR (Bennett 1962) radio galaxies decreases with redshift for  $z > 0.3$ , while the lobe propagation velocity computed on the basis from spectral aging tends to increase with redshift and radio power (see Fig. 1 in this paper and Fig. 19 in WDW97a). Also, it appears that there is no relation between radio power and lobe-lobe size at fixed redshift (see, e.g., Lacy et al. 1993; Nesser et al. 1995; Wan & Daly 1998b). Since the lobe-lobe size is proportional to the lobe propagation velocity times the lifetime, it can be inferred that high-redshift 3CR galaxies have shorter lifetimes than low-redshift sources. The higher redshift sources also have larger beam powers than the lower redshift sources since radio power and beam power are roughly proportional (Wan et al. 1996; Wan & Daly 1998b). A shorter lifetime for a more powerful source is contrary to what is expected in an Eddington-limited outflow, since the Eddington lifetime depends only upon certain efficiency factors and is independent of the beam power and the total

energy of the central compact object, though it should be noted that such an outflow could still be Eddington limited if the efficiency factors vary with the beam power.

Let the total time that an AGN produces two highly collimated oppositely directed outflows be  $t_*$ , and let the rate of growth of the radio bridges,  $v_L$ , be roughly constant over the source lifetime, which is supported by spectral aging analyses (AL87; LPR92; Daly 1994, 1995). The average or characteristic lobe-lobe size a source would have if it could be observed over its entire lifetime is  $D_* \simeq v_L t_*$ . Following Daly (1994),  $t_*$  is related to the energy extraction rate or beam power,  $L_j$ , by a power law:

$$t_* \propto L_j^{-\beta/3}. \quad (3)$$

This implies that the characteristic source size is

$$D_* \propto k L_j^{(1-\beta)/3} \propto k^\beta v_L^{1-\beta}, \quad (4)$$

where  $k = (n_a a_L^2)^{-1/3}$  (see eq. [2]). Clearly, for  $\beta = 1$ , the average source size depends only upon  $n_a$  and  $a_L$  and is independent of  $L_j$ , whereas for  $\beta > 1$ , the average source size decreases as the beam power and radio power increase.

The implications of equation (3) are far-reaching. It implies that the total energy available to power the outflow is fixed at some initial value, since  $E_i \simeq L_j t_* \propto L_j^{(1-\beta/3)}$ , assuming that  $L_j$  is roughly constant over the source lifetime which is supported by the current data (see § 2.1). Note that for  $\beta \simeq 3$ , the energy extraction rate  $L_j$  is independent of the energy  $E_i$  available to power the outflow, while for  $\beta \simeq 0$ , the beam power and AGN lifetime are independent and  $L_j \propto E_i$ , analogous to an Eddington luminosity.

In practice,  $D_*$  is estimated using the expression introduced by Daly (1994), originally referred to as  $l_*$ :

$$D_* \propto \left( \frac{1}{B_L a_L} \right)^{2\beta/3} v_L^{1-\beta/3}. \quad (5)$$

The normalization is chosen so that  $D_*$  at  $z \simeq 0$  matches the observed average lobe-lobe size for sources at this redshift that are subject to the power cut discussed in § 3.1. The magnetic field strength,  $B_L$ , in a synchrotron-emitting radio source and the lobe propagation velocity based on spectral aging (Myers & Spangler 1985),  $v_L$ , can be estimated using the field strength that minimizes the total energy in relativistic electrons and magnetic field (see, e.g., Miley 1980). The estimates of  $B_L$  and  $v_L$  can also be computed using magnetic fields systematically offset from the minimum energy field, which is discussed in detail by WDW97a and WDW97b (see § 3.2.1).

Assuming the energy density of the field in the radio bridge is large compared to that in the microwave background radiation (i.e., synchrotron losses dominate over inverse Compton losses) and a spectral index of  $\alpha = 1$  ( $S_\nu \propto \nu^{-\alpha}$ ), it can be shown that

$$D_* \propto (a_0 r)^{(4/7-2\beta/3)} (1+z)^{(23/14-5\beta/6)}, \quad (6)$$

where  $z$  is the redshift of the radio source, and  $(a_0 r)$  is the coordinate distance to the source. The value of  $\beta$  indicated by the data for all parameter choices is  $\beta \sim 2$  (see § 4.3), and for this value,  $D_* \propto (a_0 r)^{-0.8}$ . The ratio  $\langle D \rangle / D_*$ , where  $\langle D \rangle$  is the average lobe-lobe size, has a rather strong dependence on cosmological parameters via  $(a_0 r)$ :  $\langle D \rangle / D_* \propto (a_0 r)^{1.8} (1+z)^{-1}$ , for  $\beta \sim 2$ . The results presented in subsequent sections include the effects of inverse Compton scattering with microwave background photons and the

observed spectral indices, but the assumptions made above show the dependence of  $D_*$  on cosmology in one approximation.

The main hypothesis of the model is that single epoch radio data can be used to estimate the average lobe-lobe size the source would have if it could be observed over its entire lifetime, called  $D_*$ . Since very powerful FR II radio galaxies form a very homogeneous population, the average size of a given source should be close to the average size of the population at the same redshift, as discussed in detail in § 4.2. Thus, one test of the model is whether  $D_*$  tracks  $\langle D \rangle$  independent of redshift for a large sample of sources selected using similar criteria; this is shown to be the case in § 4.3. If the sources are sampled randomly during their lifetimes, the distribution of  $t/t_*$  should be redshift independent, where  $t$  is the age of the source when it is observed and  $t_*$  is the lifetime of collimated outflows; this is shown to be the case in § 4.2. Also, if the model correctly describes the data, then the ratio  $\langle D \rangle / D_*$  should exhibit much less scatter than the ratio  $D/D_*$ ; this is shown to be the case in § 4.2.

### 3. RADIO GALAXIES EXAMINED

#### 3.1. The Sample Used to Estimate $\langle D \rangle$

In order to be able to use the model described in § 2.2, the sources examined must have lobes that propagate supersonically, and have no significant backflows or bridge distortions. Thus, only FR II radio galaxies with  $P_{178}(q_0 = 0) \gtrsim 3 h^{-2} \times 10^{26} \text{ WHz}^{-1} \text{ sr}^{-1}$  are examined here (see §§ 1 and 2.1). Radio-loud quasars are not included in this work since the lobe-lobe sizes of radio-loud quasars evolve differently with redshift than radio galaxies (see, e.g., Singal 1988), their bridges are more distorted than those of radio galaxies (LMS89), and they may suffer from more serious projection effects (Wan & Daly 1998c).

The 3CR radio galaxies with Galactic latitude greater than  $10^\circ$  are completely identified, and all have spectroscopic redshifts. On the basis of published 178 MHz fluxes and spectral indices compiled by Spinrad et al. (1985), 81 radio galaxies from the list compiled by McCarthy, van Breugel, & Kapahi (1991) have  $P_{178}(q_0 = 0) \gtrsim 3 h^{-2} \times 10^{26} \text{ W Hz}^{-1} \text{ sr}^{-1}$ . These sources are used here to estimate  $\langle D \rangle$ . Cygnus A (3C 405), which is not listed by McCarthy et al. (1991) due to its low Galactic latitude ( $6^\circ$ ), is added to this sample since it is the closest high-power FR II radio galaxy ( $z = 0.056$ ), is well studied (see, e.g., Carilli et al. 1991), and is included in the  $D_*$  sample described below (§ 3.2).

Table 1 gives the mean and median lobe-lobe sizes for the high-power FR II 3CR galaxies assuming a flat, matter-dominated universe with  $(\Omega_0 = 1.0, \Omega_\Lambda = 0)$ ; an open, curvature-dominated universe with  $(\Omega_0 = 0.1, \Omega_\Lambda = 0)$ ; and a spatially flat universe with a nonzero cosmological constant  $(\Omega_0 = 0.1, \Omega_\Lambda = 0.9)$ ; here and throughout,  $\Omega_0$  refers to the ratio of the mass density to the critical value at the current epoch,  $\Omega_\Lambda$  refers to the ratio of the energy density of a cosmological constant to the critical density,  $\Omega_k = 1 - \Omega_0 - \Omega_\Lambda$  is the normalized curvature. A value of  $h = 1$  is adopted when a value must be chosen, though  $h$  scales out of many quantities, and the dependence on  $h$  is typically weak when it does enter.

Figure 1 shows the mean lobe-lobe sizes from Table 1. Excluding the lowest redshift bin, an obvious decrease in the physical size with increasing redshift can be seen for the cosmological parameters considered. Note that the lowest

TABLE 1  
LOBE-LOBE SIZES FOR  $P_{178} \gtrsim 3 h^{-2} \times 10^{26} \text{ W Hz}^{-1} \text{ sr}^{-1}$  FR II 3CR GALAXIES

BIN	z RANGE	NUMBER OF SOURCES	$\Omega_0 = 1.0, \Omega_\Lambda = 0.0$		$\Omega_0 = 0.1, \Omega_\Lambda = 0.0$		$\Omega_0 = 0.1, \Omega_\Lambda = 0.9$	
			$\langle D \rangle$ (kpc $h^{-1}$ )	$D_{\text{med}}$ (kpc $h^{-1}$ )	$\langle D \rangle$ (kpc $h^{-1}$ )	$D_{\text{med}}$ (kpc $h^{-1}$ )	$\langle D \rangle$ (kpc $h^{-1}$ )	$D_{\text{med}}$ (kpc $h^{-1}$ )
1.....	0.0–0.3	3	66 ± 14	52 ± 14	68 ± 14	55 ± 14	72 ± 13	60 ± 13
2.....	0.3–0.6	15	177 ± 42	160 ± 43	197 ± 47	175 ± 48	227 ± 54	200 ± 55
3.....	0.6–0.9	27	126 ± 18	127 ± 18	149 ± 21	147 ± 21	179 ± 25	176 ± 26
4.....	0.9–1.2	19	91 ± 21	51 ± 16	114 ± 27	63 ± 21	141 ± 33	79 ± 26
5.....	1.2–1.6	10	83 ± 30	39 ± 18	110 ± 40	51 ± 25	137 ± 50	63 ± 31
6.....	1.6–2.0	8	50 ± 17	37 ± 18	71 ± 24	53 ± 25	88 ± 30	66 ± 31

redshift, which contains Cygnus A, is not an obvious outlier in the comparison of  $D_*$  and  $\langle D \rangle$  as discussed in § 4.3 below and by Guerra & Daly (1996).

3.2. The Sample Used to Estimate  $D_*$

An estimate of  $D_*$  requires estimates of the lobe radius, the lobe magnetic field strength, and the lobe propagation velocity of the radio source (see eq. [5]). Fourteen 3CR radio galaxies have enough radio bridge data published to estimate these parameters and satisfy the power cut

described in § 2.1. Wellman & Daly (1996), WDW97a, and WDW97b reanalyzed the radio maps from LMS89 and LPR92 for their studies of the bridge structure and gaseous environments of powerful extended radio sources, and computed  $v_L$ ,  $B_L$ , and  $a_L$  for both data sets in a similar manner. Table 2 lists the 14 radio galaxies from WDW97a and WDW97b, all of which are used here. Note that since they are all high-power 3CR radio galaxies, they are all included in the larger, full high-power 3CR sample of radio galaxies, described in § 3.1. One bridge from 3C 239 was excluded by WDW97a and WDW97b because its morphology suggests sidelfow (see WDW97a and WDW97b for details). WDW97b compute values for the lobe half-width,  $a_L$ , measured  $10 h^{-1}$  kpc from the hot spot toward the host galaxy, the magnetic fields measured  $10 h^{-1}$  kpc and  $25 h^{-1}$  kpc from the hot spot toward the host galaxy, and the lobe propagation velocity,  $v_L$ , which is affected by offsets in the magnetic field from minimum energy conditions and corrections for redshift evolution of spectral index as discussed below.

3.2.1. Uncertainties that Affect Estimates of  $D_*$

The magnetic field in the radio lobe,  $B_L$ , enters into the estimate of the lobe pressure,  $P_L$ , and the magnetic field strength of the radio bridge,  $B_B$ , and  $B_L$  enter into the estimate of the lobe propagation velocity. Both values affect the estimate of the ambient gas density,  $n_a$  (WDW97b). Several observations indicate that the magnetic field strength in powerful extended radio sources is less than the minimum energy magnetic field strength. Expressing the true magnetic field as  $B = bB_{\text{min}}$ , where  $B_{\text{min}}$  is the minimum energy

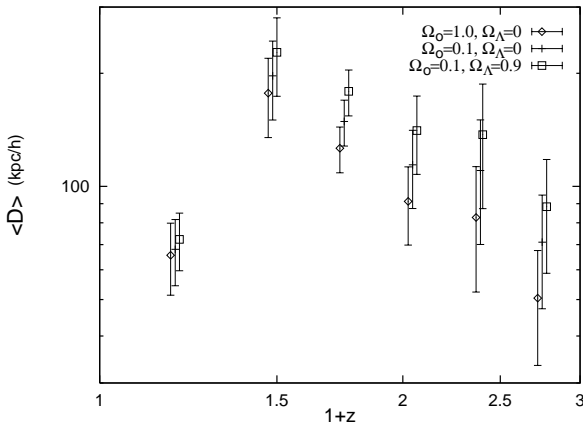


FIG. 1.—Mean lobe-lobe size  $\langle D \rangle$  vs.  $(1+z)$  for high-power,  $P_{178}(q_0 = 0) \gtrsim 3 h^{-2} \times 10^{26} \text{ W Hz}^{-1} \text{ sr}^{-1}$ , 3CR radio galaxies for three different cosmologies (see figure legend).

TABLE 2  
RADIO GALAXIES WITH  $D_*$  PRESENTED HERE

SOURCE	z	BIN	$\log [P_{178}(q=0)]$ ( $h^{-2} \text{ W Hz}^{-1} \text{ sr}^{-1}$ )	$\theta$ (arcsec)	MAP REFERENCE	$r_*^b$		$D_*^b$ (kpc $h^{-1}$ )
						(kpc $h^{-1}$ )	(kpc $h^{-1}$ )	
3C 405.....	0.056	1	27.39	127	LMS	32 ± 3	36 ± 4	68 ± 5
3C 330.....	0.549	2	27.01	62	LMS	82 ± 13	92 ± 12	174 ± 18
3C 427.1.....	0.572	2	27.08	23	LMS	49 ± 5	67 ± 8	116 ± 9
3C 55.....	0.720	3	27.26	71	LMS	73 ± 10	101 ± 17	174 ± 20
3C 247.....	0.749	3	26.89	16.7	LPR	88 ± 13	97 ± 12	185 ± 17
3C 265.....	0.811	3	27.33	78	LMS	82 ± 14	100 ± 17	182 ± 22
3C 289.....	0.967	4	27.28	11.8	LPR	58 ± 6	53 ± 5	112 ± 8
3C 268.1.....	0.974	4	27.46	46	LMS	70 ± 8	63 ± 7	133 ± 10
3C 280.....	0.996	4	27.60	17.7	LPR	52 ± 6	64 ± 6	116 ± 8
3C 356.....	1.079	4	27.43	75	LMS	81 ± 16	50 ± 10	131 ± 18
3C 267.....	1.144	4	27.58	38	LMS	54 ± 9	51 ± 7	105 ± 11
3C 68.2.....	1.575	5	27.85	22	LMS	111 ± 29	70 ± 10	181 ± 31
3C 322.....	1.681	6	27.84	33	LMS	37 ± 4	47 ± 8	84 ± 9
3C 239.....	1.790	6	28.15	13.0	LPR	43 ± 4	<sup>a</sup>	87 ± 6

<sup>a</sup>  $r_*$  for only one bridge.

<sup>b</sup> Computed assuming  $B = 2.0, \Omega_0 = 0.1, \Omega_\Lambda = 0.4, b = 0.25$ , and not including  $\alpha$ -z correction.

magnetic field, Carilli et al. (1991) find that  $b = 0.3$  in order for ram pressure confinement of the lobes of Cygnus A to be consistent with X-ray measurements of the ambient gas density. Perley & Taylor (1991) find a similar value for 3C 295 based on ram pressure confinement of the lobes, while Feigelson et al. (1995) and Kaneda et al. (1995) find similar values for Fornax A by comparing the radio emission with X-rays produced by inverse Compton scattering of microwave background photons with the relativistic electrons that produce the radio emission. WDW97a use three independent and complementary methods to estimate  $b$  in Cygnus A, and their results agree with the Carilli et al. (1991) result. WDW97b also show that the source to source dispersion in  $b$  must be small, less than about 15%. However, both  $b = 0.25$  and  $b = 1.0$  cases are examined below for completeness (§ 4.3, Tables 3–5).

Another uncertainty that affects  $D_*$  is whether the evolution of the radio spectral index with redshift introduces a systematic error on the lobe propagation velocity. It has been noted for some time that the radio spectral index of the 3CR sample and of other samples increases systematically with redshift; this could be due to spectral curvature or due to other causes (see, e.g., Röttgering et al. 1994). The radio spectral index is an important ingredient in estimating the lobe propagation velocity via the effects of spectral aging of relativistic electrons. Though it should be noted that for  $\beta \sim 2$ , which is indicated by the data independent of systematic effects on the lobe propagation velocity (§ 4.3),  $D_* \propto (a_L B_L)^{-4/3} v_L^{1/3}$ , which is a fairly weak dependence on  $v_L$ . It is not clear whether the data should be corrected for the systematic increase of the radio spectral index with redshift. This correction, referred to as the  $\alpha$ - $z$  correction, does not change the low-redshift velocities, but decreases the high-redshift velocities by, at most, a factor of 2 (see WDW97a, Fig. 19). Results obtained both with and without the  $\alpha$ - $z$  correction are examined below (§ 4.3, Tables 3–5).

#### 4. EXAMINING THE MODEL

##### 4.1. Computed $D_*$ Values

Each bridge has a characteristic core-lobe length,  $r_* \simeq D_*/2$ , where  $D_*$  is obtained using equation (5) and inputting the values of  $v_L$ ,  $a_L$ , and  $B_L$  from each bridge. Note that one can estimate  $D_*$  using the average of the input parameters in equation (5) over both bridges or by adding  $r_*$  for both

bridges. Both methods would be equivalent if the sources were completely symmetric, but the latter method accounts for any slight asymmetry in these sources and is used here. As an example for one set of parameter choices, Table 2 lists  $r_*$  computed using the results for the radio galaxies from WDW97b and assuming  $b = 0.25$  without the  $\alpha$ - $z$  correction, ( $\Omega_0 = 0.1$ ,  $\Omega_\Lambda = 0$ ), and  $\beta = 2.0$ . This example is chosen because ( $\Omega_0 = 0.1$ ,  $\Omega_\Lambda = 0$ ) is the moderate choice of the three example cosmologies introduced in Table 1, and  $\beta = 2.0$  is the value of  $\beta$  indicated by the data for all parameter choices (§ 4.3). Estimates of  $D_*$  throughout this paper are computed by adding both  $r_*$  values, except for 3C 239, which has  $r_*$  for only one bridge and has  $D_*$  set equal to twice the available  $r_*$ . The normalization of  $D_*$  is chosen so that the ratio of the lobe-lobe  $D_*$  for Cygnus A (3C 405) to  $\langle D \rangle$  for the lowest redshift bin is unity.

Figure 2a shows  $D_*$  as a function of  $(1+z)$  assuming ( $\Omega_0 = 0.1$ ,  $\Omega_\Lambda = 0$ ),  $b = 0.25$  without the  $\alpha$ - $z$  correction, and  $\beta = 0.0$ , which is indicative of an Eddington-limited system; Figure 2b shows the same except it is assumed that  $\beta = 2.0$  which is the value indicated by the data for all parameter choices in § 4.3. In these figures and all other figures in this work, diamonds represent radio galaxies from the LMS89 sample, and stars represent radio galaxies from the LPR92 sample. These figures show that  $D_*$  estimates for LMS89 and LPR92 sources agree well with each other for the range of  $\beta$  considered, although the two samples are more similar for  $\beta = 2$  than for  $\beta = 0$ . Note that the LPR92 sources have smaller angular extent than the LMS89 sources (Table 2), and have smaller lobe-lobe sizes, which implies they are younger (see § 4.2 below). The fact that the smaller sources from LPR92 and the larger sources from LMS89 give consistent  $D_*$  at similar redshifts indicates that the model discussed in § 2.2 is yielding a characteristic length that is independent of when the source is observed during its lifetime.

Figure 2a shows that  $D_*$  increases as redshift increases for  $\beta = 0.0$ , which differs from the redshift dependence of the average lobe-lobe sizes (see Fig. 1). Figure 2b shows that, ignoring the lowest redshift bin (Cygnus A),  $D_*$  decreases with increasing redshift for  $\beta = 2.0$ . The general trend is that increasing  $\beta$  makes the slope of  $D_*$  versus  $(1+z)$  decrease (i.e., become more negative) excluding the lowest redshift bin. Thus, for  $\beta = 2.0$ , the redshift behavior of  $D_*$  tracks that of  $\langle D \rangle$ .

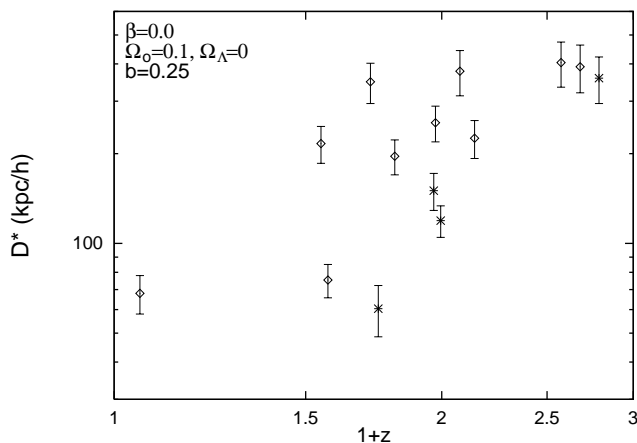


FIG. 2a

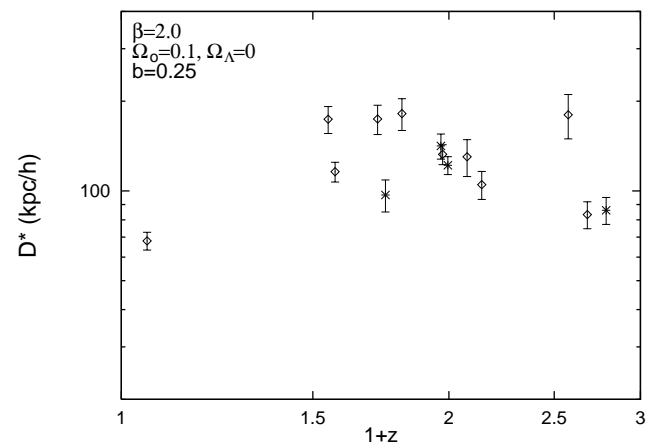


FIG. 2b

FIG. 2.—Characteristic length  $D_*$  vs.  $(1+z)$  computed without the  $\alpha$ - $z$  correction, and assuming  $\Omega_0 = 0.1$ ,  $\Omega_\Lambda = 0$ , and  $b = 0.25$  for two choices of  $\beta$ : (a)  $\beta = 0.0$  and (b)  $\beta = 2.0$ . Diamonds represent LMS89 sources, and stars represent LPR92 sources.

For  $\beta = 0.0$ ,  $D_*$  for 3C 427.1 ( $z = 0.572$ ) is similar to the  $D_*$  value for Cygnus A ( $z = 0.056$ ), while for  $\beta = 2.0$ ,  $D_*$  for 3C 427.1 is similar to those for the rest of the  $0.3 < z < 0.6$  sources. Excluding this source slightly decreases, by about 0.3, estimates of  $\beta$  (see § 4.3). Cygnus A ( $z = 0.056$ ) has low values for  $D_*$  when compared with most sources in the redshift interval  $0.3 < z < 0.9$ . This is intriguing since  $\langle D \rangle$  has a relatively low value in the lowest redshift bin and tracks the redshift behavior of  $D_*$  when Cygnus A is included (see Fig. 1). Excluding Cygnus A does not affect the estimates of  $\beta$  but slightly affects estimates of  $\Omega_0$  using this data set (see Guerra & Daly 1996 § 4.3).

#### 4.2. Comparing $D$ to $D_*$

The observed lobe-lobe size of a powerful extended radio source is  $D \simeq 2v_L t$ , where  $t$  is the age of the source when observed, and  $v_L$  is the lobe propagation velocity which is assumed to be roughly constant over the lifetime of a source. An alternate way of expressing the size for a given source is

$$D = 2 \left( \frac{t}{t_*} \right) D_* . \quad (7)$$

In a given redshift range ( $z - \delta z$  to  $z + \delta z$ ) of a sample of radio sources, the distribution of  $D_*$  values should be peaked around some central value  $D_{*z}$  in a given redshift range ( $z - \delta z$  to  $z + \delta z$ ). Taking the values of  $D_*$  in this redshift range to be equal to the constant  $D_{*z}$ , the mean lobe-lobe size is

$$\langle D \rangle = 2 \left\langle \left( \frac{t}{t_*} \right) D_* \right\rangle \simeq 2 \left\langle \frac{t}{t_*} \right\rangle D_{*z} . \quad (8)$$

If we assume for a given sample that the distribution of  $t/t_*$ , the fraction of a source's lifetime at which it is observed, is randomly distributed between zero and unity, then  $\langle D \rangle \simeq D_{*z}$ . More generally, if the  $t/t_*$  distribution of a sample does not depend on redshift, then  $\langle D \rangle \propto D_{*z}$ , and the ratio  $\langle D \rangle / D_{*z}$  should be constant and independent of redshift. It is this premise that allows an estimate of  $\beta$  and cosmological parameters.

Figure 3 shows the ratio of the physical size  $D$  to the characteristic size  $D_*$  for the sample of radio galaxies examined here, assuming  $b = 0.25$  and not including the  $\alpha$ - $z$  correction. In Figure 3, ( $\Omega_0 = 0.1$ ,  $\Omega_\Lambda = 0.0$ ) is assumed since it is the moderate choice of the three example cosmologies in Table 1, and  $\beta = 2.0$  is assumed since it is the value indicated by the data for all other parameter choices (see 4.3). Since equation (7) gives  $t/t_* \propto D/D_*$  for a given source with constant  $v_L$ , the sample shows no significant  $t/t_*$  redshift evolution. Fitting  $D/D_* = a(1+z)^n$  we obtain  $a = 1.15 \pm 0.07$  and  $n = -0.04 \pm 0.09$ ; similar results are found for  $b = 1.0$  and including the  $\alpha$ - $z$  correction. Thus, the data are consistent with the sources being observed at random times during their lifetimes. The reduced  $\chi^2$  of the fit is 41, which is due to the large scatter of  $D/D_*$ . It should be noted that the scatter in  $D/D_*$  is much greater than that of  $\langle D \rangle / D_*$  (see Fig. 8b), which indicates that though the sources are sampled over a broad range of fractional ages, sources at a given redshift yield similar  $D_*$ .

#### 4.3. Constraints Obtained by Comparing $\langle D \rangle$ to $D_*$ at a Given Redshift

A quantitative constraint on the parameter  $\beta$  may be obtained by fitting the ratio  $\langle D \rangle / D_*$  to a constant, indepen-

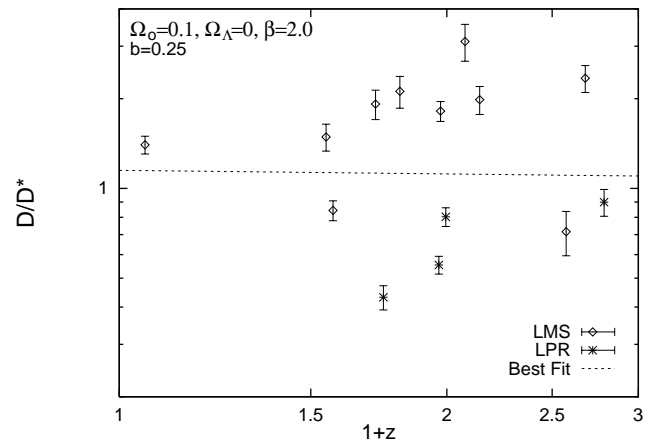


FIG. 3.— $D/D_*$  vs.  $(1+z)$ , assuming  $\Omega_0 = 0.1$ ,  $\Omega_\Lambda = 0$ , and  $\beta = 2.0$ , for  $b = 0.25$  without the  $\alpha$ - $z$  correction. Since  $v_L$  is assumed constant over the lifetime of a source,  $D/D_* \propto t/t_*$ . Diamonds represent LMS89 sources, and stars represent LPR92 sources. The dashed line is the best fit to a power law.

dent of redshift and finding the value of  $\beta$  that minimizes the reduced  $\chi^2$ . Table 3 lists the values of  $\beta$  that minimize the reduced  $\chi^2$ ,  $\beta_{\min}$ , for ( $\Omega_0 = 1.0$ ,  $\Omega_\Lambda = 0$ ), ( $\Omega_0 = 0.1$ ,  $\Omega_\Lambda = 0$ ), and ( $\Omega_0 = 0.1$ ,  $\Omega_\Lambda = 0.9$ ). Four cases are examined in Table 3: (A),  $b = 0.25$  without the  $\alpha$ - $z$  correction; (B),  $b = 0.25$  with the  $\alpha$ - $z$  correction; (C),  $b = 1.0$  without the  $\alpha$ - $z$  correction; and (D),  $b = 1.0$  with the  $\alpha$ - $z$  correction. Error estimates for the fitted parameters here and throughout are the 68% confidence intervals that correspond to the regions of the parameter space within which the  $\chi^2$  value increases by no more than 1.0 from the minimum value (see, e.g., Press et al. 1992, § 15.6). Although the errors that enter into computing the  $\chi^2$  value may not be Gaussian, we shall assume Gaussian errors as a rough approximation in order to use the  $\chi^2$  value as an estimate of errors for fitted parameters. The  $\beta_{\min}$ 's from Table 3 are all consistent within  $2\sigma$  for all the cases (A–D) and the three cosmologies examined. A range of about 1.5–2.6 is found for  $\beta_{\min}$ .

Figures 4a and 4b show contour plots of the reduced  $\chi^2$  as a function of  $\beta$  and  $\Omega_0$ , for case A described above, assuming  $\Omega_\Lambda = 0$  and  $\Omega_k = 0$ , respectively. It is clear from these figures that the constraints on  $\beta$  are not significantly affected by the assumed cosmology, and a consistent range of  $\beta_{\min}$  from 1.5 to 2.75 emerges. Most significantly,  $\beta = 0$  gives a reduced  $\chi^2$  value of just slightly greater than 6, for all cosmologies shown. Thus, taken at face value, the data are not consistent with Eddington-limited outflows in powerful extended radio sources. Contour plots for the cases B, C, and D described above are also shown in Figures 5, 6, and 7, respectively. The constraints on  $\beta$  are not significantly different for the four cases (A–D) examined, and all cases give a high reduced  $\chi^2$  value, greater than 3, for  $\beta = 0$ . Note that these figures only depict the range of  $\Omega_0$  from 0 to 1, but fits have been extended outside this range, including  $\Omega_0 < 0$ , which gives divergent values of the coordinate distance,  $(a_0 r)$ , for  $k = 0$  (see Table 4).

Table 4 shows the best-fit values of  $\Omega_0$  and  $\beta$  for a constant  $\langle D \rangle / D_*$  independent of redshift. The fits for  $\Omega_0$  vary by about 0.2–0.4 depending on the case (A–D) described above, which follows from Figures 4–7. A value of  $\Omega_0$  less than unity is indicated by these fits for all parameter choices, and  $\Omega_0 = 1$  is inconsistent at about the  $2\sigma$  level. These constraints on  $\Omega_0$  are very similar to those placed using supernovae as a modified standard candle, which

TABLE 3  
BEST-FIT  $\beta_{\min}$  AND  $\chi^2_{\text{red}}$  HOLDING  $\langle D \rangle / D_*$  CONSTANT, INDEPENDENT OF  $z$

CASE <sup>a</sup>	$\Omega_0 = 1.0, \Omega_\Lambda = 0.0$		$\Omega_0 = 0.1, \Omega_\Lambda = 0.0$		$\Omega_0 = 0.1, \Omega_\Lambda = 0.9$	
	$\beta_{\min}$	$\chi^2_{\text{red}}$	$\beta_{\min}$	$\chi^2_{\text{red}}$	$\beta_{\min}$	$\chi^2_{\text{red}}$
A .....	$2.60 \pm 0.35$	1.05	$2.30 \pm 0.30$	0.67	$2.10 \pm 0.30$	0.69
B .....	$2.00 \pm 0.35$	1.84	$2.00 \pm 0.30$	1.17	$1.95 \pm 0.30$	1.07
C .....	$2.35 \pm 0.40$	0.95	$2.10 \pm 0.35$	0.67	$1.90 \pm 0.35$	0.82
D .....	$1.70 \pm 0.30$	1.37	$1.75 \pm 0.30$	1.00	$1.75 \pm 0.35$	1.11

<sup>a</sup> Refers to cases as follows: (A),  $b = 0.25$  without  $\alpha$ - $z$  correction; (B),  $b = 0.25$  with  $\alpha$ - $z$  correction; (C),  $b = 1.0$  without  $\alpha$ - $z$  correction; (D),  $b = 1.0$  with  $\alpha$ - $z$  correction.

indicate that  $\Omega_0$  has a low value about  $2 \sigma$  away from 1 (Perlmutter et al. 1997; Garnavich et al. 1997), are in agreement with results from dynamical estimates of cluster densities (Lin et al. 1996; Carlberg et al. 1997), and are as strong a constraint as those from studies of large-scale velocity fields which indicate that  $\Omega_0 > 0.3$  (see, e.g., Dekel et al. 1993; Dekel & Rees 1994; Hudson et al. 1995). The use of powerful extended radio galaxies to constrain cosmological parameters is discussed further in § 5 below.

Table 5 shows the results of fitting  $\langle D \rangle / D_*$  to a power law in  $(1+z)$ ,  $\langle D \rangle / D_* \propto (1+z)^p$ . A value of  $p = 0$  is expected for the correct parameter choices (see § 4.2). Best-fit values for  $\beta$  and  $p$  are shown for the four cases described above (A–D) and three choices of cosmological parameters.

It is interesting to note that the fits for  $\beta$  converge to similar values for different cosmologies when a power-law fit is allowed. The fits in which  $(\Omega_0 = 1.0, \Omega_\Lambda = 0)$  are the only ones that give a significantly nonzero value of  $p$ , in which case  $p$  is about  $2 \sigma$  less than zero. Figures 8a, 8b, and 8c show the ratio  $\langle D \rangle / D_*$  and the best fit to a constant (the weighted mean in log-space), assuming  $b = 0.25$  without the  $\alpha$ - $z$  correction and  $\beta = 2.0$ , for  $(\Omega_0 = 1.0, \Omega_\Lambda = 0)$ ,  $(\Omega_0 = 0.1, \Omega_\Lambda = 0)$ , and  $(\Omega_0 = 0.1, \Omega_\Lambda = 0.9)$ , respectively. The slopes found in the power-law fits for  $(\Omega_0 = 1.0, \Omega_\Lambda = 0)$  are apparent in Figure 8a and can be explained by the incorrect choice of cosmological parameters. This implies that if the universe is flat and matter-dominated, then there is some redshift evolution that has not been accounted for.

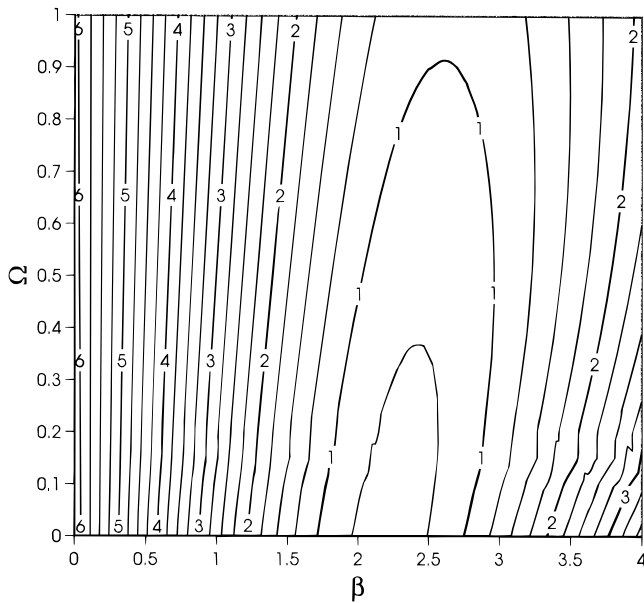


FIG. 4a

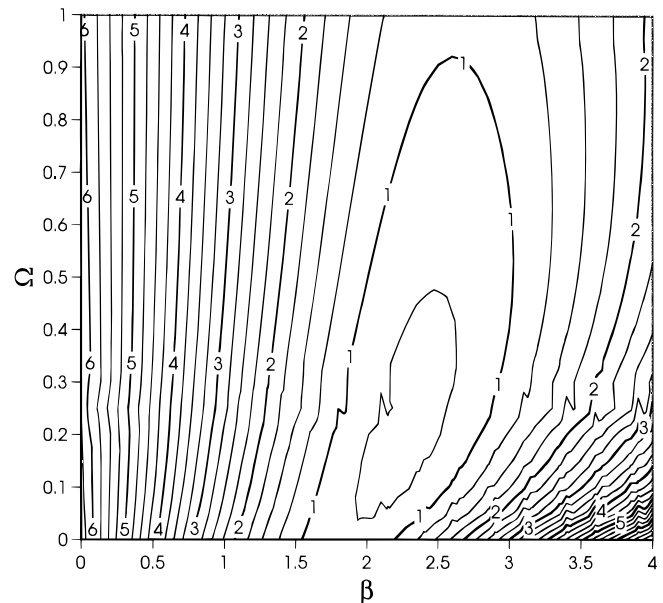


FIG. 4b

FIG. 4.—The reduced  $\chi^2$  as a function of  $\beta$  and  $\Omega_0$  obtained by fitting  $\langle D \rangle / D_*$  to a constant, independent of redshift, assuming  $b = 0.25$  and no  $\alpha$ - $z$  correction: (a) for  $\Omega_\Lambda = 0$  and (b)  $\Omega_k = 0$ . Integer values of the reduced  $\chi^2$  are labeled in figures; the contours increase in steps of 0.25, with the lowest contour at a reduced  $\chi^2$  of 0.75. Note that the reduced  $\chi^2 = 1$  contour translates to a  $\sigma$  of about 2 for both figures, assuming Gaussian errors.

TABLE 4  
BEST-FIT  $\Omega_0$ ,  $\beta_{\min}$ , AND  $\chi^2_{\text{red}}$  FITTING  $\langle D \rangle / D_*$  TO A CONSTANT, INDEPENDENT OF  $z$

CASE <sup>a</sup>	$\Omega_\Lambda = 0$			$k = 0, \Omega_\Lambda = 1 - \Omega_0$		
	$\Omega_0$	$\beta_{\min}$	$\chi^2_{\text{red}}$	$\Omega_0$	$\beta_{\min}$	$\chi^2_{\text{red}}$
A .....	$-0.10^{+0.50}_{-0.40}$	$2.15 \pm 0.30$	0.65	$0.20^{+0.30}_{-0.20}$	$2.25 \pm 0.30$	0.67
B .....	$-0.35^{+0.30}_{-0.25}$	$1.75 \pm 0.25$	0.95		$\Omega_0 < 0$	
C .....	$0.10^{+0.50}_{-0.35}$	$2.10 \pm 0.35$	0.67	$0.35^{+0.35}_{-0.30}$	$2.25 \pm 0.35$	0.69
D .....	$-0.05^{+0.45}_{-0.30}$	$1.75 \pm 0.30$	0.98	$0.20^{+0.35}_{-0.30}$	$1.80 \pm 0.35$	1.07

<sup>a</sup> Refers to cases as follows: (A),  $b = 0.25$  without  $\alpha$ - $z$  correction; (B),  $b = 0.25$  with  $\alpha$ - $z$  correction; (C),  $b = 1.0$  without  $\alpha$ - $z$  correction; (D),  $b = 1.0$  with  $\alpha$ - $z$  correction.

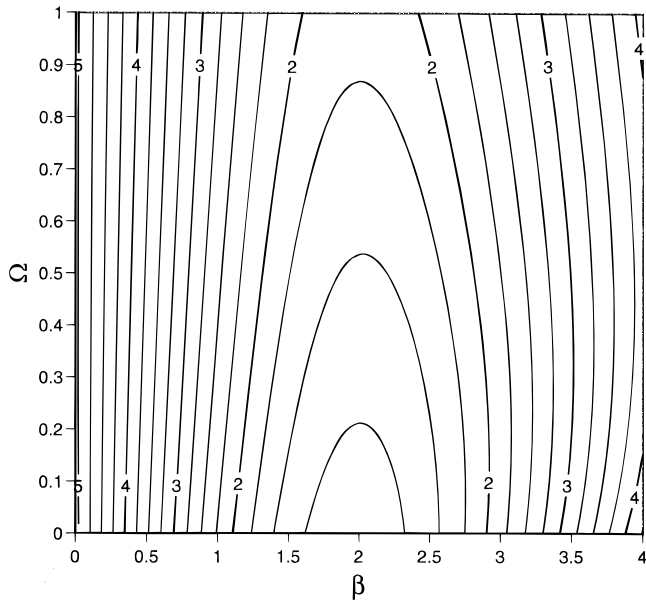


FIG. 5a

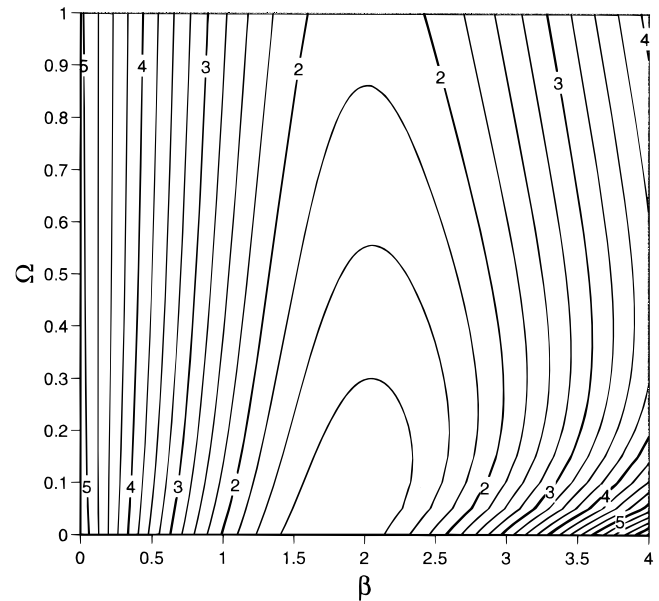


FIG. 5b

FIG. 5.—The reduced  $\chi^2$  as a function of  $\beta$  and  $\Omega_0$  obtained by fitting  $\langle D \rangle / D_*$  to a constant, independent of redshift, assuming  $b = 0.25$  and with the  $\alpha$ - $z$  correction: (a) for  $\Omega_\Lambda = 0$  and (b)  $\Omega_k = 0$ . Integer values of the reduced  $\chi^2$  are labeled in figures; the contours increase in steps of 0.25, with the lowest contour at a reduced  $\chi^2$  of 1.25. Note that the reduced  $\chi^2 = 1.5$  contour translates to a  $\sigma$  of about 2 for both figures, assuming Gaussian errors.

The possibility that certain sources in the  $D_*$  sample may not be representative of powerful extended radio sources at their respective redshifts was considered (Guerra 1997). For example, the only low-redshift source for which we have an estimate of  $D_*$  is Cygnus A (3C 405,  $z = 0.056$ ); perhaps Cygnus A is an unusual source. A source that is similar to Cygnus A in many respects, including size, lobe propagation velocity, surrounding ambient gas density, and ambient gas temperature, is 3C 427.1 (WDW97a, WDW97b). Also, two sources, 3C 68.2 and 3C 239, do not seem to follow the predictions of adiabatic bridge expansion, according to WDW97a. All of the analyses described above have been repeated while excluding different combinations of these sources (3C 405, 3C 427.1, 3C 68.2, and 3C 239), and the

differences are negligible except for a slight reduction of  $\beta_{\min}$  by about 0.3 when 3C 427.1 is excluded holding all other parameters fixed. The reduction of  $\beta_{\min}$  when 3C 427.1 is excluded occurs because lower  $\beta$  tends to make 3C 427.1 an outlier (see Figs. 2a and 2b).

The data give an estimate of  $\beta$  that is insensitive to virtually all other parameter choices and data cuts. A reasonable estimate of  $\beta$  is  $\beta = 2.1 \pm 0.6$  based on Figures 4–7 and Tables 3–5. It is safe to state that  $\beta$  must be between 1 and 3 and that these outflows are not Eddington limited,  $\beta \neq 0$ . The main conclusion that can be drawn about cosmological parameters is that a flat, matter-dominated universe ( $\Omega_0 = 1.0$ ,  $\Omega_\Lambda = 0$ ) is about  $2 \sigma$  away from the best-fit values (see § 5 below).

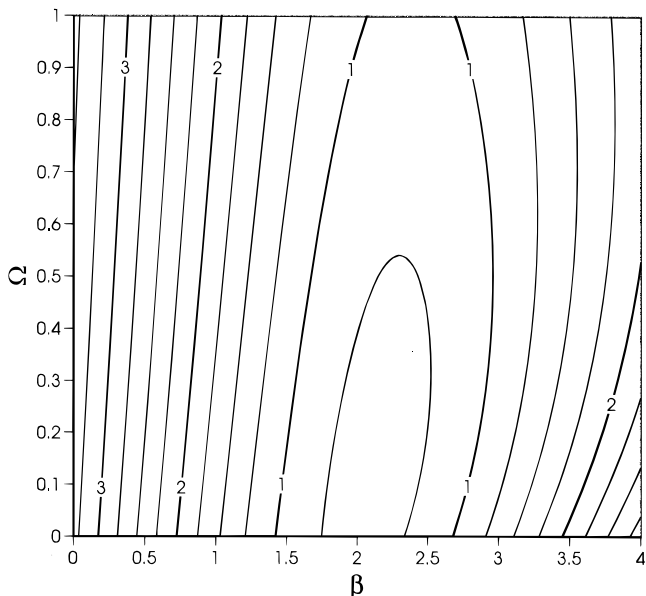


FIG. 6a

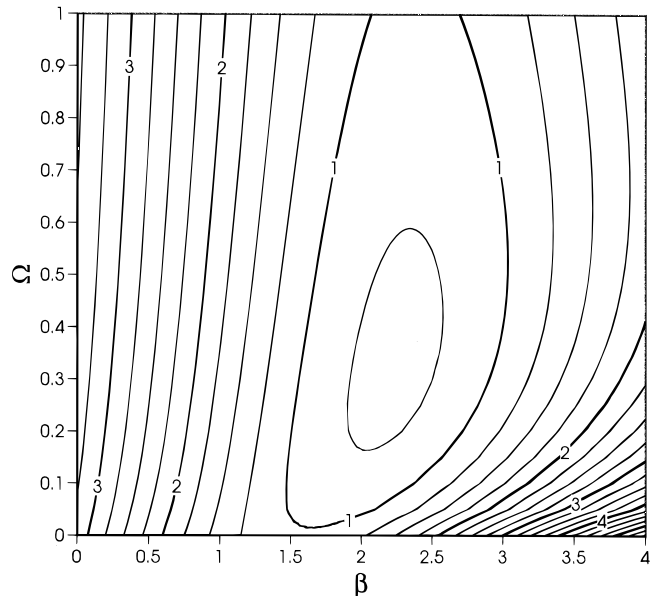


FIG. 6b

FIG. 6.—The reduced  $\chi^2$  as a function of  $\beta$  and  $\Omega_0$  obtained by fitting  $\langle D \rangle / D_*$  to a constant, independent of redshift, assuming  $b = 1.0$  and no  $\alpha$ - $z$  correction: (a) for  $\Omega_\Lambda = 0$  and (b)  $\Omega_k = 0$ . Integer values of the reduced  $\chi^2$  are labeled in figures; the contours increase in steps of 0.25, with the lowest contour at a reduced  $\chi^2$  of 0.75. Note that the reduced  $\chi^2 = 1$  contour translates to a  $\sigma$  of about 2 for both figures, assuming Gaussian errors.

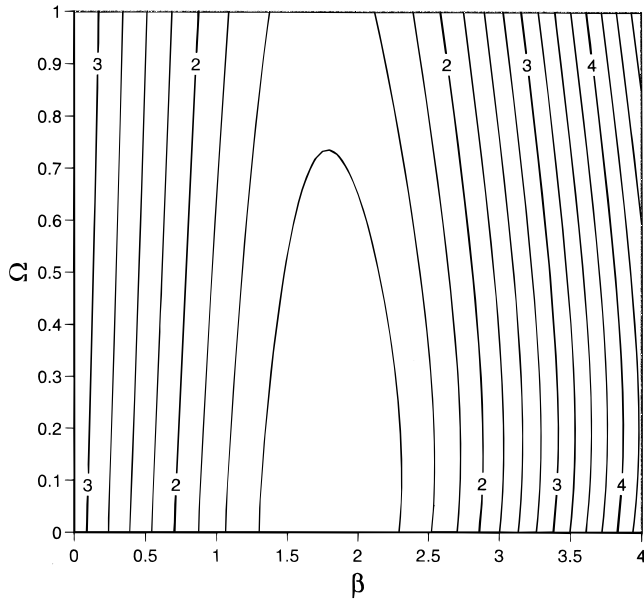


FIG. 7a

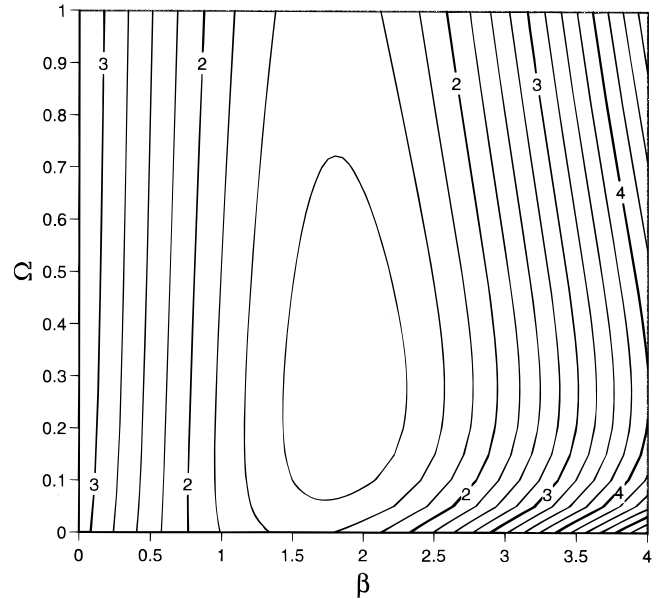


FIG. 7b

FIG. 7.—The reduced  $\chi^2$  as a function of  $\beta$  and  $\Omega_0$  obtained by fitting  $\langle D \rangle / D_*$  to a constant, independent of redshift, assuming  $b = 1.0$  and with  $\alpha$ - $z$  correction: (a) for  $\Omega_\Lambda = 0$  and (b)  $\Omega_k = 0$ . Integer values of the reduced  $\chi^2$  are labeled in figures; the contours increase in steps of 0.25, with the lowest contour at a reduced  $\chi^2$  of 1.25. Note that the reduced  $\chi^2 = 1.5$  contour translates to a  $\sigma$  of about 2 for both figures, assuming Gaussian errors.

#### 5. CAN POWERFUL EXTENDED RADIO SOURCES BE USED FOR COSMOLOGY?

In order to be able to use the model outlined in § 2.2 to estimate cosmological parameters, accurate estimates of  $a_L$ ,  $B_L$ , and  $v_L$  are needed (see eq. [5]). Though two inputs to  $v_L$  are not completely understood at this time, it is still interesting to apply the method to this data set and consider all possible effects on  $v_L$  to see the implications for cosmological parameters.

One factor that is not completely understood is the offset of magnetic field strength from the minimum energy value. This enters as a scaling factor of  $B_L$  and affects only the redshift behavior of  $D_*$  through the redshift behavior of  $v_L$ . It turns out that the dependence of  $D_*$  on  $v_L$  is rather weak for  $\beta \sim 2$  (see eq. [5]):  $D_* \propto (a_L B_L)^{-4/3} v_L^{1/3}$ , but the effect of the offset from minimum energy conditions on  $v_L$  is considered nonetheless. As the magnetic field strength decreases from the minimum energy value, the role of inverse Compton cooling begins to become important relative to the role of synchrotron cooling in these sources. The effects of both types of cooling on the radio spectral index are used to estimate spectral ages, and thus  $v_L$ . As discussed by WDW97b, for  $b = 0.25$ , the two cooling mechanisms are of comparable importance for many sources at high redshift. This offset affects both the redshift behavior of the  $v_L$

(shown in Fig. 4 of WDW97b) and the dependence of  $D_*$  on  $(a_0 r)$ , the coordinate distance to the source.

The second effect that may change estimates of the lobe propagation velocity is the increase of the radio spectral index with redshift. It is not clear whether the data should be corrected to account for the observed systematic increase of the radio spectral index with redshift (discussed in detail by WDW97b). For 3CR radio galaxies,  $v_L$  increases with redshift, as do the radio power and the radio spectral index. This increase is well known and has been noted by many authors. If, for example, the initial radio spectrum is not a power law but has some curvature (see, e.g., Röttgering et al. 1994), the observed spectral index should be corrected for the observed redshift evolution as was done for the  $\alpha$ -corrected data (WDW97b). On the other hand, if the correlation is not due to, or only partly due to, spectral curvature, then such a correction is not appropriate.

To account for these two uncertainties, both  $b = 0.25$  and  $b = 1$  are considered, and both  $\alpha$ - $z$ -corrected and  $\alpha$ - $z$ -uncorrected velocities are considered (see § 4.3). The results are not strongly dependent on these changes (see Table 4), as expected since  $D_* \propto v_L^{1/3}$ . The effect of using a value of  $b = 1.0$  instead of  $b = 0.25$  is to increase the best fit  $\Omega_0$  by about 0.2, and the effect of including the corrections to spectral index is to lower the best-fit  $\Omega_0$  by about 0.2 (see Table 4). A precise fit for  $\Omega_0$  cannot be made until the

TABLE 5  
BEST-FIT  $\beta_{\min}$ ,  $p(\beta_{\min})$ , AND  $\chi_{\text{red}}^2$  SETTING  $\langle D \rangle / D_* = C(1+z)^p$

CASE <sup>a</sup>	$\Omega_0 = 1.0, \Omega_\Lambda = 0.0$			$\Omega_0 = 0.1, \Omega_\Lambda = 0.0$			$\Omega_0 = 0.1, \Omega_\Lambda = 0.9$		
	$\beta_{\min}$	$p(\beta_{\min})$	$\chi_{\text{red}}^2$	$\beta_{\min}$	$p(\beta_{\min})$	$\chi_{\text{red}}^2$	$\beta_{\min}$	$p(\beta_{\min})$	$\chi_{\text{red}}^2$
A .....	$2.25 \pm 0.35$	$-0.75 \pm 0.30$	0.74	$2.20 \pm 0.35$	$-0.15 \pm 0.30$	0.71	$2.30 \pm 0.35$	$0.30 \pm 0.30$	0.70
B .....	$1.85 \pm 0.35$	$-0.95 \pm 0.30$	1.18	$1.85 \pm 0.35$	$-0.40 \pm 0.30$	1.11	$1.90 \pm 0.35$	$-0.05 \pm 0.25$	1.15
C .....	$2.20 \pm 0.40$	$-0.60 \pm 0.30$	0.76	$2.15 \pm 0.40$	$0.05 \pm 0.30$	0.72	$2.25 \pm 0.40$	$0.50 \pm 0.30$	0.71
D .....	$1.75 \pm 0.35$	$-0.60 \pm 0.30$	1.16	$1.75 \pm 0.35$	$-0.05 \pm 0.30$	1.08	$1.80 \pm 0.35$	$0.30 \pm 0.30$	1.11

<sup>a</sup> Refers to cases as follows: (A),  $b = 0.25$  without  $\alpha$ - $z$  correction; (B),  $b = 0.25$  with  $\alpha$ - $z$  correction; (C),  $b = 1.0$  without  $\alpha$ - $z$  correction; (D),  $b = 1.0$  with  $\alpha$ - $z$  correction.

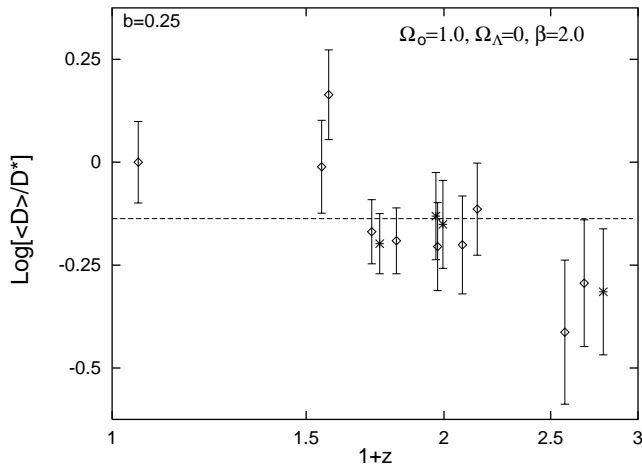


FIG. 8a

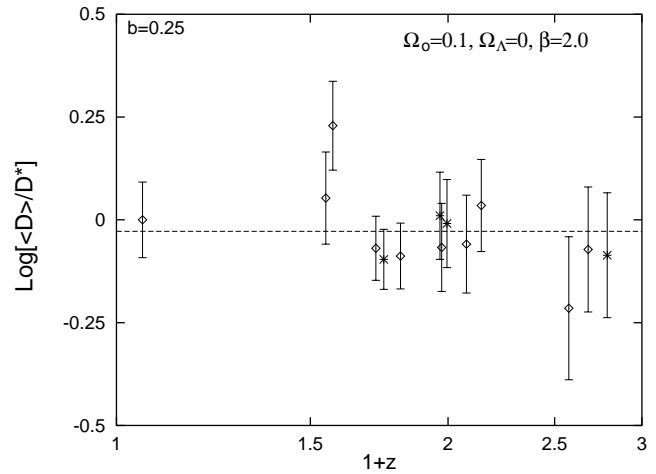


FIG. 8b

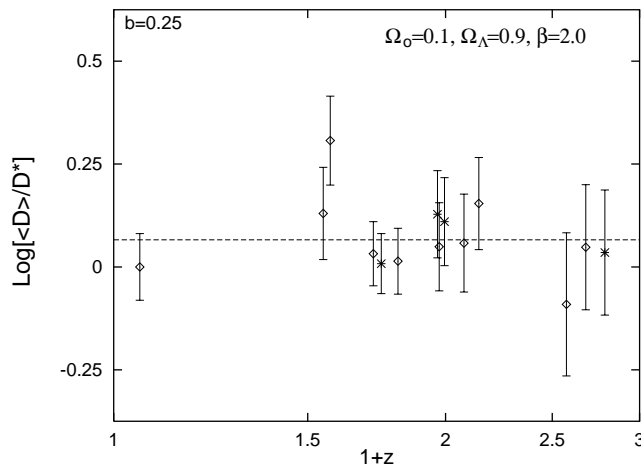


FIG. 8c

FIG. 8.—  $\langle D \rangle / D_*$  vs.  $(1+z)$ , assuming  $\beta = 2.0$ ,  $b = 0.25$ , for three choices of cosmology: (a) ( $\Omega_0 = 1.0$ ,  $\Omega_\Lambda = 0$ ), (b) ( $\Omega_0 = 0.1$ ,  $\Omega_\Lambda = 0$ ), and (c) ( $\Omega_0 = 0.1$ ,  $\Omega_\Lambda = 0.9$ ). Diamonds represent LMS89 sources, and stars represent LPR92 sources. The dashed line is the weighted mean in log-space of all  $\langle D \rangle / D_*$  in the figure, assuming  $\langle D \rangle / D_*$  is redshift independent.

parameters that are varied between the four cases (A–D) described in § 4.3 are known. However, the current range of  $\Omega_0$  allowed can be discussed.

An ideal solution to the uncertainties described above would be to identify an independent estimate of the lobe propagation velocity for all or some of these sources. This could be compared with the lobe propagation velocity estimated using the spectral aging model used here. The velocity can be independently estimated if either the ambient gas temperature or the ambient gas density can be estimated. WDW97a have shown that the geometrical shape of the radio bridge may be used to estimate the Mach number of the lobe, so the combination of the Mach number and the ambient gas temperature can be used to estimate the lobe propagation velocity. Perhaps observations by *AXAF* will be used to measure the ambient gas temperature since its spatial resolution and spectral coverage could allow it to separate X-rays produced by the AGN from those produced by thermal bremsstrahlung from the hot ambient gas. Daly (1994, 1995) and WDW97b have shown that the lobe propagation velocity and lobe pressure may be used to estimate the ambient gas density; if the ambient gas density can be estimated independently, the lobe pressure and ambient gas density may be combined to solve for the lobe propagation velocity. Studies of the gaseous environments of these

sources using the Sunyaev-Zeldovich effect or high-resolution *AXAF* measurements may lead to independent estimates of the ambient gas density, which may be combined with the lobe pressure to solve for the lobe propagation velocity.

## 6. DISCUSSION

A relation between the active lifetime during which an AGN produces a highly collimated outflows,  $t_*$ , and the beam power,  $L_j$ , is introduced that can reconcile the observed evolution of radio source size with redshift, and the independence of radio source size and radio power at a given redshift for powerful extended radio sources (see § 2.2). What emerges from this model is a characteristic length scale,  $D_*$ , that can be thought of as the lobe-lobe size averaged over a source's lifetime, which can be predicted from measurable quantities such as the lobe width, the lobe propagation velocity, and the lobe magnetic field strength.

The model parameter  $\beta$ , which relates  $t_*$  and  $L_j$ , is estimated by comparing the redshift evolution of  $D_*$  to that of the average lobe-lobe sizes for powerful extended radio galaxies. For all the cases and cosmologies considered, a consistent range of  $\beta$  emerges (§ 4.3). The best-fit values allow  $\beta$  to range from about 1.5 to 2.75, so a good rough estimate of  $\beta$  is  $2.1 \pm 0.6$ . This is consistent with the range of

$\beta = 1.5 \pm 0.5$  obtained by Daly (1994, 1995).

These data are not consistent with  $\beta = 0$ , which is expected for an Eddington-limited system ( $t_*$  independent of  $L_j$  as discussed in § 2.2). In Figure 2a, where  $\beta = 0.0$  is assumed, the  $D_*$  estimates are clearly increasing with redshift, which is opposite to the evolution of  $\langle D \rangle$  for the high-power 3CR sample described in § 3.1. The data are best fitted with  $\beta > 1.0$ , which yield reduced  $\chi^2$  values less than 1.5, whereas fits assuming  $\beta = 0$  yield reduced  $\chi^2$  values greater than 3 (see Figs. 4–7). The values of  $\beta$  obtained here imply that  $D_*$  should decrease for increasing  $L_j$  or  $v_L$  (see § 2.2), which is consistent with the redshift evolution of the average sizes of high-power 3CR sources (Fig. 1), and the redshift evolution of  $L_j$  and  $v_L$  (discussed by Wan & Daly 1997b). A value of  $\beta \sim 3$  implies that the beam power is independent of the energy available to power the outflow.

A flat, matter-dominated universe ( $\Omega_0 = 1.0$ ,  $\Omega_\Lambda = 0$ ) is allowed at about the  $2\sigma$  level for the full range of parameter allowed. It should be noted that the constraints on  $\Omega_0$  obtained here are very similar to the constraints placed using supernovae as a modified standard candle which indicate  $\Omega_0$  has a low value about  $2\sigma$  away from one (Perlmutter et al. 1997; Garnavich et al. 1997), are in agreement with results from dynamical estimates of cluster den-

sities (Lin et al. 1996; Carlberg et al. 1997), and are as strong a constraint as those obtained from the study of the large-scale velocity fields (see, e.g., Dekel et al. 1993; Dekel & Rees 1994; Hudson et al. 1995). Stronger cosmological constraints can be placed using this method when the lobe propagation velocity can be more accurately determined, as discussed in § 5, or can be measured directly by comparing X-ray temperature measurements with the shape of the radio bridge, as described by WDW97a, or by comparing the X-ray density or Sunyaev-Zeldovich pressure with the pressure of the radio lobe, as described by WDW97b.

Special thanks go to Greg Wellman and Lin Wan for access to their results and valuable discussions. The authors would also like to thank Mitch Begelman, Roger Blandford, Dave De Young, George Djorgovski, Stephen Eales, Ed Groth, Paddy Leahy, Simon Lilly, Alan Marscher, George Miley, Colin Norman, Jerry Ostriker, Lyman Page, Jim Peebles, Rick Perley, Tony Readhead, Martin Rees, Brigitte Rocca, David Schramm, Rashid Sunyaev, and Dave Wilkinson for helpful discussions. This work was supported in part by the US National Science Foundation, by a NSF Graduate Fellowship, the Independent College Fund of New Jersey, and by a grant from W. M. Wheeler III.

#### REFERENCES

- Alexander, J. P., & Leahy, J. P. 1987, *MNRAS*, 225, 1 (AL87)  
 Bennett, A. S. 1962, *MmRAS*, 68, 163  
 Blandford, R. A., & Payne, D. G. 1982, *MNRAS*, 199, 883  
 Blandford, R. A., & Znajek, R. L. 1977, *MNRAS*, 179, 433  
 Carilli, C. L., Perley, R. A., Dreher, J. W., & Leahy, J. P. 1991, *ApJ*, 383, 554  
 Carlberg, R. G., Morris, S. L., Yee, H. K. C., & Ellingson, E. 1997, *ApJ*, 479, L19  
 Daly, R. A. 1990, *ApJ*, 355, 416  
 ———, 1994, *ApJ*, 426, 38  
 ———, 1995, *ApJ*, 454, 580  
 Dekel, A., Bertschinger, E., Yahil, A., Strauss, M. A., Davis, M., & Huchra, J. P. 1993, *ApJ*, 412, 1  
 Dekel, A., & Rees, M. J. 1994, *ApJ*, 422, L1  
 Eilek, J. A. 1996, in *ASP Conf. Proc. 100, Energy Transport in Radio Galaxies and Quasars*, ed. P. Hardee, A. Bridle, & A. Zensus (San Francisco: ASP), 73  
 Eilek, J. A., & Arendt, P. N. 1996, *ApJ*, 457, 150  
 Fanaroff, B. L., & Riley, J. M. 1974, *MNRAS*, 167, 31  
 Feigelson, E. D., Laurent-Muehleisen, S. A., Kollgaard, R. I., & Fomalont, E. B. 1995, *ApJ*, 449, L149  
 Garnavich, P. M., et al. 1997, preprint  
 Guerra, E. J. 1997, Ph.D. thesis, Princeton Univ.  
 Guerra, E. J., & Daly, R. A. 1995, in *Cygnus A: Study of a Radio Galaxy*, ed. C. Carilli & D. Harris (Cambridge: Cambridge University Press), 252  
 Harris, D. E., Carilli, C. A., & Perley, R. A. 1994, *Nature*, 367, 713  
 Hudson, M. J., Dekel, A., Courteau, S., Faber, S. M., & Willick, J. A. 1995, *MNRAS*, 274, 305  
 Kaneda, H., et al. 1995, *ApJ*, 453, L13  
 Katz-Stone, D. M., Rudnick, L., & Anderson, M. 1993, *ApJ*, 407, 549  
 Lacy, M., Rawlings, S., Saunders, R., & Warner, P. J. 1993, *MNRAS*, 264, 721  
 Leahy, J. P., Muxlow, T. W., & Stephens, P. W. 1989, *MNRAS*, 239, 401 (LMS89)  
 Leahy, J. P., & Williams, A. G. 1984, *MNRAS*, 210, 929 (LW84)  
 Lightman, A. P., & Eardley, D. M. 1974, *ApJ*, 187, L1  
 Lin, H., et al. 1996, *ApJ*, 471, 617  
 Liu, R., Pooley, G., & Riley, J. M. 1992, *MNRAS*, 257, 545 (LPR92)  
 McCarthy, P. J., van Breugel, W., & Kapahi, V. K. 1991, *ApJ*, 371, 478  
 Miley, G. 1980, *ARA&A*, 18, 165  
 Myers, S. T., & Spangler, S. R. 1985, *ApJ*, 291, 52  
 Narayan, R., & Yi, I. 1994, *ApJ*, 428, L13  
 ———, 1995, *ApJ*, 444, 231  
 Neeser, M. J., Eales, S. A., Law-Green, J. D., Leahy, J. P., & Rawlings, S. 1995, *ApJ*, 451, 76  
 Norman, M. L. 1996, in *ASP Conf. Proc. 100, Energy Transport in Radio Galaxies and Quasars*, ed. P. Hardee, A. Bridle, & J. Zensus (San Francisco: ASP), 319  
 Perley, R. A., & Taylor, G. B. 1991, *AJ*, 101, 1623  
 Perlmutter, S., et al. 1997, preprint  
 Press, W. H., Teukolsky, S. A., Vetterling, W. T., & Flannery, B. P. 1992, *Numerical Recipes in C* (Cambridge: Cambridge Univ. Press)  
 Rees, M. J., Begelman, M. C., Blandford, R. D., & Phinney, E. S. 1982, *Nature*, 295, 17  
 Ro7ttgering, H. J. A., Lacy, M., Miley, G. K., Chambers, K. C., & Saunders, R. 1994, *A&AS*, 108, 79  
 Rudnick, L., & Katz-Stone, D. M. 1996, in *Cygnus A: Study of a Radio Galaxy*, ed. C. Carilli & D. Harris (Cambridge: Cambridge Univ. Press), 158  
 Rudnick, L., Katz-Stone, D. M., & Anderson, M. 1994, *ApJS*, 90, 955  
 Singal, A. K. 1988, *MNRAS*, 233, 870  
 Spinrad, H., Djorgovski, S., Marr, J., & Aguilar, L. A. 1985, *PASP*, 97, 932  
 Wan, L., & Daly, R. A. 1998a, *ApJ*, in press  
 ———, 1998b, *ApJS*, in press  
 ———, 1998c, *ApJ*, submitted  
 Wan, L., Daly, R. A., & Wellman, G. F. 1996, in *ASP Conf. Proc. 100, Energy Transport in Radio Galaxies and Quasars*, ed. P. Hardee, A. Bridle, & J. Zensus (San Francisco: ASP), 305  
 Wellman, G. F., & Daly, R. A. 1996, in *Cygnus A: Study of a Radio Galaxy*, ed. C. Carilli & D. Harris (Cambridge: Cambridge University Press), 246  
 Wellman, G. F., Daly, R. A., & Wan, L. 1997a, *ApJ*, 480, 79 (WDW97a)  
 ———, 1997b, *ApJ*, 480, 96 (WDW97b)  
 Wilson, A. C., & Colbert, E. J. M. 1995, *ApJ*, 438, 62